Intensities and Intensity Statistics

4

4.1 Intensity Expressions and Factors Affecting Intensities

The measurement of the intensity of a diffracted X-ray beam can be carried out photographically by camera methods, but almost always today by quantum counting with diffractometer techniques. We can measure either a peak intensity or an integrated intensity, the latter parameter being preferred for the expression of the intensity of X-ray reflection.

Real crystals are not geometrically perfect, so that a given reflection will be observed over a small, finite angular range. Hence, we need to be able to determine the area under a curve such as that shown in Fig. 4.1 in order to represent a total intensity of a reflection. In the photographic method, the peak intensity is recorded over a grid of points and the integrated result imposed onto a photographic film. In collecting intensities with a diffractometer, a scintillation counter sweeps through a pre-set angular range $\pm\delta\theta_0$, so recording the total number of counts, or integrated intensity. We shall discuss some of the practical implications of these techniques in the next chapter, but much of the ensuing discussion in this chapter will have the collection of intensity data by an X-ray diffractometer and its subsequent treatment in mind.

The total energy of a given diffraction spectrum $\mathcal{E}(hkl)$ at any given angle θ_0, for a crystal sufficiently small that absorption may be neglected, and completely bathed in an X-ray beam and rotating with a uniform angular velocity ω, is given for unpolarized incident radiation of incident intensity I_0, by

$$\mathcal{E}(hkl)\omega/I_0 = Q\delta v \tag{4.1}$$

where $\mathcal{E}(hkl)\omega/I_0$ is known as the *integrated reflection*, δv is the volume of the crystal, and Q is given by

$$Q = (N^2\lambda^3/\sin 2\theta_0)|\mathrm{F}(hkl)|^2[e^2/(4\pi\varepsilon_0 m_e c^2)^2(1+\cos^2 2\theta_0)/2] \tag{4.2}$$

where N is the number of unit cells per unit volume of the crystal, and the other terms have their conventional meanings. The derivation of these expressions has been discussed in detail elsewhere [1].

Since the value of the integrated reflection does not actually depend upon the angular velocity, we let $R(\theta)I_0$ be the radiation reflected at the angle θ_0 by the crystal, so that $R(\theta)$ may be called the reflecting power. Then,

M. Ladd and R. Palmer, *Structure Determination by X-ray Crystallography: Analysis by X-rays and Neutrons*, DOI 10.1007/978-1-4614-3954-7_4,

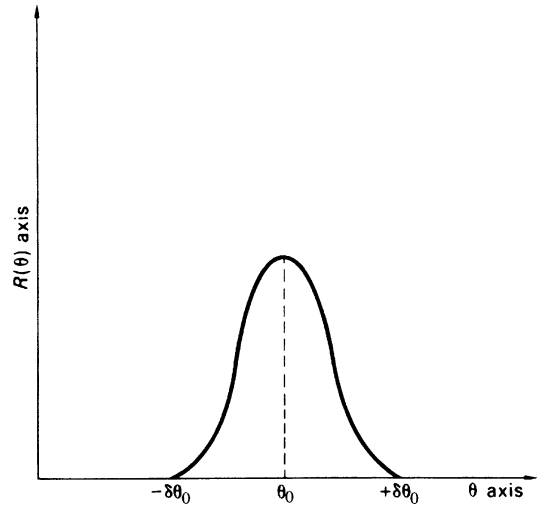

Fig. 4.1 Variation of reflection power $R(\theta)$ with θ; the intensity at the Bragg angle θ_0 is recorded over the angular range $\pm\delta\theta_0$

$$\mathcal{E} = \int R(\theta) I_0 / \omega \, \mathrm{d}\theta$$

so that

$$\mathcal{E}\omega / I_0 = \int R(\theta) \, \mathrm{d}\theta = Q\delta v \tag{4.3}$$

The term $\int R(\theta) \, \mathrm{d}\theta$ expresses the area under the curve in Fig. 4.1. From (4.2), we can write

$$\mathcal{E}\omega / I_0 = KC(hkl)(1/\sin 2\theta)\frac{1}{2}(1 + \cos^2 2\theta)|\mathrm{F}(hkl)|^2 \tag{4.4}$$

where K is a scaling factor and $C(hkl)$ is a factor that depends upon absorption and extinction, both of which we shall discuss shortly. Essentially, the area under the curve of Fig. 4.1 may be expressed as

$$\int R(\theta) \, \mathrm{d}\theta = KC(hkl)Lp|\mathrm{F}(hkl)|^2 \tag{4.5}$$

where the L and p are the trigonometrical terms in (4.4), to be discussed next.

4.1.1 Polarization and Lorentz Factors

In (4.5), L and p represent the Lorentz and polarization factors, respectively, thus linking the quantity measured, the reflecting power, to the quantity sought, the corrected $|\mathrm{F}(hkl)|^2$ value, which we may refer to as the *ideal intensity*.

The polarization factor p, discussed in Sect. 3.2.4, takes into account the fact that the output of a conventional X-ray tube is unpolarized radiation, whereas the radiation after reflection from a crystal plane is polarized, thus decreasing the intensity of the diffracted beam as a function of the scattering angle 2θ.

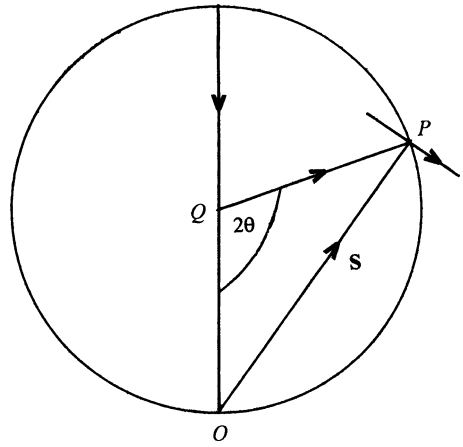

Fig. 4.2 Lorentz factor: sphere of reflection with the crystal at its center Q; O is the origin of the reciprocal lattice, P is a reciprocal lattice point hkl in the position for a reflection from the corresponding plane. The distance OP is $|\mathbf{S}|$, and the normal to it represents the velocity vector of P; $\angle QOP = \angle QPO = (90 - \theta)^\circ$

Where the incident beam is polarized, for example, after reflection from a crystal monochromator, the polarization factor is modified to $(1 + \cos^2 2\theta \cos^2 2\theta_m)/(1 + \cos^2 2\theta_m)$, where $2\theta_m$ is the angle between the incident and scattered beams at the monochromator.

The Lorentz factor L depends on the diffraction geometry and expresses a *time-of-reflection opportunity* for a crystal plane in the X-ray beam. For a rotating crystal with the X-ray beam normal to a reflecting plane the L factor is $1/(\sin 2\theta)$; with a powder specimen it takes the form $2/(\sin\theta \sin 2\theta)$.

In order to give expression to the Lorentz factor in a particular case, let P be a point on a zero level of the reciprocal lattice, normal to a rotation axis that passes through its origin O; the crystal is at Q and the incident X-ray beam direction is QO, as shown in Fig. 4.2. The constant angular velocity of the crystal is ω, so that the reciprocal lattice point P has a linear velocity $|\mathbf{S}|\omega$. The speed with which P moves through the surface of the Ewald sphere is the component of its velocity along the radius QP. Since $\angle QOP = \angle QPO = (90 - \theta)^\circ$, the velocity v of the point P as it passes through the sphere is given by

$$v = \omega |\mathbf{S}| \cos\theta \tag{4.6}$$

Since $|\mathbf{S}| = 2\sin\theta/\lambda$, the velocity v is equal to $(\omega/\lambda) \sin 2\theta$. The time t taken for P to pass through the reflecting position is proportional to $1/v$, so that this time-of-reflection is given by

$$t = k/v = k/(\omega |\mathbf{S}| \cos\theta) \tag{4.7}$$

where k is a constant depending on both the size of the reciprocal lattice, in practice, the wavelength of X-radiation, and the limits $\pm\delta\theta$ for finite reflection. The denominator in (4.7) depends on the time-of-reflection opportunity for the given crystal plane; it is the Lorentz factor when the rotation axis is normal to the reflecting plane. From (4.6), $\omega/v = 1/(|\mathbf{S}| \cos\theta)$, so that

$$L = \omega/v = \lambda/(2\sin\theta \cos\theta) = \lambda/(\sin 2\theta) \tag{4.8}$$

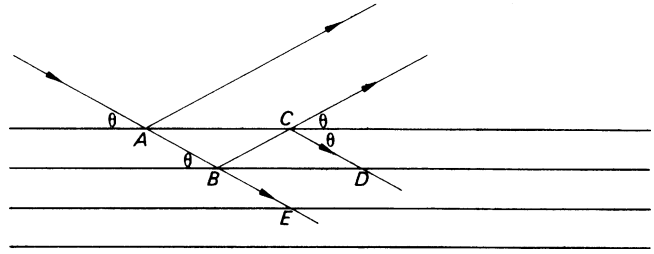

Fig. 4.3 Primary extinction: the phase changes by reflection at B and C are each $\pi/2$, so that between the directions BE and CD, the total phase change is π. Thus, there is an attenuation of the incident X-ray beam reaching planes deeper into the crystal

Since both ω and λ remain constant, L is equal to $1/\sin 2\theta$ for the given experimental arrangement. This argument assumes $\kappa = 1$; if $\kappa = \lambda$, $S = 2 \sin \theta$, and the same result obtains.

4.1.2 Extinction

We consider a crystal bathed in the X-ray beam, under the conditions for normal Bragg reflection, with all unit cells stacked together in a regular manner. Figure 4.3 shows a family of planes, all in the same orientation θ with respect to the X-ray beam. It is clear that the first-reflected ray BC is in the correct orientation for a second reflection CD, and so on. Since there is always an inherent phase change of $\pi/2$ on reflection, the doubly reflected ray CD has a phase difference of π with respect to the incident ray AB. We note in passing that the phase change of π is neglected in crystal-structure calculations since it occurs equally for all reflections.

Primary Extinction

In general, rays that are reflected n and $(n - 2)$ times differ in phase by π, so that the net result is a reduction in intensity of the incident X-ray beam and, hence, in the diffracted beam in passing through the crystal. Energy is effectively conserved in this process, because each beam is depleted in energy by scattering into another beam, while being enhanced in energy by that which is scattered into the beam itself from other beams [2]. This effect is termed *primary extinction*, but it is very much reduced if the crystal is not perfect in its stacking. In fact, very few crystals are perfect: they are composed of an array of slightly misaligned blocks, constituting the so-called *mosaic character* of the crystal, Fig. 4.4. The ranges of geometric perfection are generally very small, less than about 10^{-3} mm, and even crystals that show primary extinction possess some mosaic character. For the ideally perfect crystal, $I \propto |F|$, whereas for the ideally imperfect crystal, $I \propto |F|^2$. Since perfection is rare and very difficult to produce in a specimen, the imperfect state with $I \propto |F|^2$ is the normal state in X-ray crystallography.

Primary extinction is most noticeable with low-order, high-intensity reflections and, if it is suspected, its effect may be very substantially reduced by the thermal shock occasioned by dipping the crystal in liquid air, thereby increasing the imperfection of the mosaic structure of the crystal.

Secondary Extinction

In Sect. 3.1.3, we considered the absorption of X-rays by materials, a process that is quite independent of the mechanism of diffraction. However, under Bragg reflection another feature may arise with an attendant attenuation of the energy of the incident X-ray beam; this effect is known as *secondary extinction*.

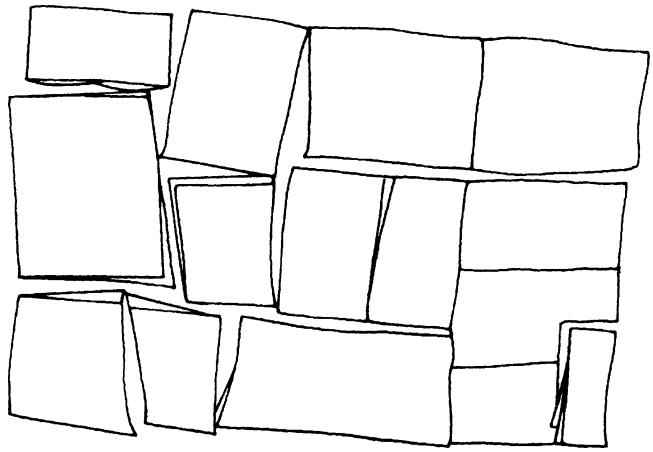

Fig. 4.4 Mosaic character in a crystal: the angular misalignment between blocks may vary from 2 to 30 min of arc

Consider a situation in which the first of a set of parallel planes encountered by the X-ray beam reflects a high proportion of the incident X-ray beam. Then, planes in this set deeper into the crystal receive less incident intensity, so that they reflect less than would be expected. The effect is most noticeable with large crystals and intense, often low-order, reflections. Crystals that have a high degree of imperfection generally show very little secondary extinction, because only a relatively small number of planes in the set are in the exact reflecting position at a given time. The ideally imperfect crystal shows least secondary extinction, and often only a few very strong reflections are affected, and they will not materially affect the structure determination. Nevertheless, it is possible to bring secondary extinction into a least-squares refinement in terms of an additional variable, the *extinction parameter* ζ; see Sect. 8.4. The quantity then minimized in the refinement of the atomic and scale parameters is

$$\sum_{hkl} w[F_o - (1/K\zeta)|F_c|]^2 \tag{4.9}$$

where F_o is the observed and $|F_c|$ the calculated structure factor amplitudes.

4.1.3 Absorption Measurement and Correction

Here we consider how the intensity may be corrected for absorption in obtaining a value for the ideal intensity $|F(hkl)|^2$.

From (3.4), the *transmission factor* T for an X-ray beam through a crystal is given by

$$T = I/I_0 = \exp[-\mu(t_i - t_d)] \tag{4.10}$$

where t_i and t_d are path lengths through the crystal for the incident and diffracted beams, respectively. If the shape of the crystal is known exactly, then it is possible to correct for absorption:

$$T = (1/V)\int_V \exp[-\mu(t_i + t_d)]\,dV \tag{4.11}$$

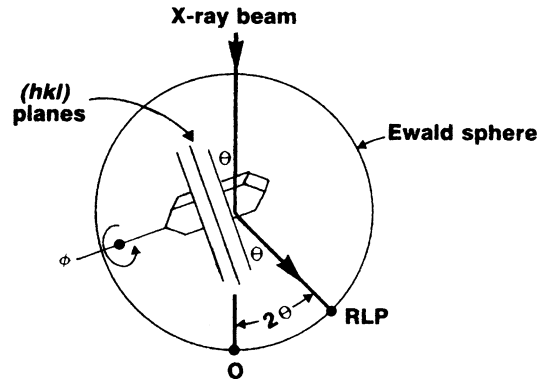

Fig. 4.5 Geometry of the empirical absorption correction: the crystal rotates on the ϕ-circle of a diffractometer with the χ-circle at $\pm 90°$

where dV is an infinitesimal portion of the volume V of the crystal [3]. Frequently, however, the crystal faces are not sufficiently well defined for this method, and an empirical procedure may be preferred.

Empirical Absorption Correction with Diffractometer Data
An empirical absorption correction is easily applied to data collected with a diffractometer, Sect. 5.5ff. Consider Fig. 4.5: the incident and diffracted X-rays for a general reflection with $\phi = \phi_0$ will intersect the transmission profile at $\phi_0 - \delta$ and $\phi_0 + \delta$, where

$$\delta = \tan^{-1}(\tan\theta \cos\chi)$$

Hence, $\delta = 0$ at $\chi = \pm 90°$. The transmission profile used is that with θ nearest to the appropriate equi-inclination angle v where

$$v = \sin^{-1}(\sin\theta \sin\chi)$$

The transmission factor T is given either as the arithmetic mean or as the geometric mean of the estimated incident and reflected ray transmissions:

$$T = [T_v(\phi - \delta) + T_v(\phi + \delta)]/2 \quad \text{or} \quad T = [T_v(\phi - \delta)T_v(\phi + \delta)]^{1/2} \tag{4.12}$$

Transmission Profiles
The transmission is measured for axial reflections, $\chi = 90°$, as a function of ϕ, Fig. 4.5. The transmission is given by

$$T_\theta(\phi) = I_\theta(\phi)/I_\theta(\max) \tag{4.13}$$

The variation of T with θ is neglected as it has the same effect as a small isotropic temperature factor. A set of profiles of T as a function of ϕ is obtained for different values of θ, and applied in data processing as detailed above.

Absorption Correction with Area Detector Data

The empirical method just described requires single Bragg reflections to be isolated and scanned so as to produce absorption correction curves. This procedure is not possible with intensity data collected with an area detector, Sect. 5.7, and other methods for applying absorption corrections have been developed. One commonly used procedure [4] uses a least-squares method to model an empirical transmission surface as sampled by multiple symmetry-equivalent and/or azimuth rotation-equivalent intensity measurements. The fitting functions are sums of real spherical harmonics of even order:

$$Y_{lm}[-\mathbf{u}(0)] + Y_{lm}[-\mathbf{u}(1)] \quad (2 \leq l = 2n \leq 8)$$

The arguments of the functions are the components of unit direction vectors, $-\mathbf{u}(0)$ relating to the reverse incident beam and $-\mathbf{u}(1)$ to the scattered beam, with respect to crystal-fixed Cartesian axes. The procedure had been verified against standard absorption correction data.

4.1.4 Scaling

Fluctuations in the incident X-ray beam intensity and possible radiation damage to the crystal may be monitored on a diffractometer by measuring four standard reflections of moderate intensity at regular intervals, say, hourly. Two of these reflections should have χ-values of approximately 0°, and two with χ near 90°, with each pair approximately 90° apart in ϕ. The average of these intensities relative to the average of their starting values is smoothed and used to rescale the raw intensity data. If S is this scale factor, different from the scale factor K applied to F_o, then the measured intensity $I_{o,meas}$ is corrected to the intensity $I_{o,corr}$:

$$I_{o,corr} = I_{o,meas}(Lp)^{-1}T^{-1}S^{-1} \tag{4.14}$$

with an estimated standard deviation given by

$$\sigma(I_{corr}) = \sigma I_{meas}(Lp)^{-1}T^{-1}S^{-1} \tag{4.15}$$

4.1.5 Merging Equivalent Reflections

Where more than the symmetry-independent region of weighted reciprocal space is measured for any given reflection, a weighted mean intensity is calculated:

$$\bar{I} = \sum_j w_j I_j \Big/ \sum_j w_j \tag{4.16}$$

where the sum is over all n measured symmetry-equivalent values of the given reflection, and w_j is given by

$$w_j = \sigma_j^{-2} \tag{4.17}$$

A chi-squared test may be used to detect equivalents that have a systematic error:

$$\chi^2 = \sum_j [(I_j - \bar{I}_j)/\sigma_j]^2 \tag{4.18}$$

where the sum is again over n symmetry-equivalent reflections and the number of degrees of freedom is $(n - 1)$. If χ^2 exceeds χ^2_{n-1} at a probability level of 0.001, then the symmetry-equivalent reflection with the highest weighted deviation from the mean, $w_j(I_j - \bar{I}_j)$, is rejected and the test repeated on the remaining equivalents. If $n = 2$, the smaller intensity value is rejected. The merging R_{int} value[1] is defined by

$$R_{\text{int}} = \sum_{hkl} \left(\sum_j |I_j - \bar{I}_j| \right) \Big/ \sum_{hkl} \left(\sum_j I_j \right) \tag{4.19}$$

4.1.6 Practical Intensity Expression and its Standard Deviation

We have developed the necessary theory to express the intensity of a reflection and the corrections that need to be applied to it in order to obtain the ideal intensity. A measurement of intensity involves values for both the intensity of the reflection, over a range $\pm\delta\theta_0$, and the background. These parameters are measured in diffractometry, by a step-scan moving-window method [5]. The standard deviation $\sigma(I)$ in I arising from statistical fluctuations is given by

$$\sigma(I) = (I + rB + r^2B)^{1/2} \tag{4.20}$$

where r is the ratio of the time spent in measuring the intensity I to that spent in measuring the background B; typically a value of r is 1.5.

We now express the ideal intensity in a practical form, assuming the absence of primary extinction, as

$$|\mathrm{F}(hkl)|^2 = I(hkl)T^{-1}S^{-1}L^{-1}p^{-1} \tag{4.21}$$

where $I(hkl)$ represents the intensity of the hkl reflection that has been adjusted for fluctuations in the incident X-ray beam, corrected for the background B and merged with symmetry-equivalent reflections, then further corrected for absorption (and extinction) T, for scaling S, and for Lorentz L, and polarization p factors, to give ideal intensity values on a correct *relative* scale, with standard deviations $\sigma(I)$.

All the corrections to intensity values that we have considered so far have been concerned with adjustments to the experimentally measured expression of the intensity of reflection. There are other related correcting factors, one of which is the secondary extinction parameter which has already been discussed; the scale factor for F_{o}, that is actually applied to $|\mathrm{F_c}|$ *during refinement*, and the temperature factors are considered next.

[1] Elsewhere, R_{int} is also called R_{m}, R_{merge} and R_{eq}.

4.1.7 Scale Factor for F_o

In the initial stage of a structure analysis, the scaling factor K for F_o can be calculated by Wilson's method, which we describe more fully in the context of intensity statistics, in Sect. 4.2.1. We write the scaling factor K in terms of F_o and $|F_c|$ as

$$|F_c| = KF_o \tag{4.22}$$

and a simplistic calculation of K during a structure analysis is evidently

$$K = \sum_{hkl} |F_c| \Big/ \sum_{hkl} F_o \tag{4.23}$$

where the sums are taken over all data for which F_o and $|F_c|$ are available. Normally, K is adjusted in a least-squares refinement, where the scale factor is applied inversely to $|F_c|$, as indicated in (4.9).

4.1.8 Thermal Vibrations and the Temperature Factor

The picture of a crystal with a total of j atoms in fixed positions with coordinates x_j, y_j, z_j needs to be modified to take into account their motion arising from the vibrational thermal energy that the atoms possess at any finite temperature. Bonding forces permit small degrees of random, relative movement of atoms, dependent upon the temperature, so that a crystal contains atoms that are vibrating about their mean positions.

The effect of thermal vibration is that the electron density is smeared out over a finite volume, rather than being concentrated at the atomic sites. Since the frequencies of vibrations are low relative to the time taken for an X-ray beam to traverse a crystal under normal experimental conditions, the crystal may be pictured as a time average of atoms randomly displaced from their mean positions, and this condition is imposed upon the diffraction pattern of the crystal.

Thermal Vibration in One Dimension

Consider first a one-dimensional periodic arrangement of scattering centers in a row of repeat distance a, and let the jth scattering species of mean fractional position x_j be displaced by a small, absolute distance u_j. Since all unit cells in this structure are not identical, the structure factor $F(h)$, using (3.63) in the x dimension alone, is given by the time and space average

$$\begin{aligned} F(h) &= \sum_j f_j \overline{\exp[i2\pi h(x_j + u_j/a)]} \\ &= \sum_j f_j \overline{\exp(i2\pi h u_j/a)} \exp(i2\pi h x_j) \end{aligned} \tag{4.24}$$

Since the displacements u_j are small, the exponential term may be expanded to three terms and, remembering that for the symmetrical vibrations of simple harmonic motion $\overline{u_j} = 0$, the average value of $\exp(i2\pi h u_j/a)$ is approximately $(1 - 2\pi^2 h^2 \overline{u_j^2}/a^2)$ to the third term, expressed conveniently, and to the same approximation, as $\exp(1 - 2\pi^2 h^2 \overline{u_j^2}/a^2)$. In the one-dimensional analysis, $h/a = 2 \sin\theta/\lambda$; hence, from (4.23), we obtain

$$\mathrm{F}(h) = \sum_j f_{j,\theta} \exp(-8\pi^2 \overline{u_j^2} \lambda^{-2} \sin^2\theta) \exp(\mathrm{i}2\pi h x_j) \tag{4.25}$$

The factor $\exp(-8\pi^2 \overline{u_j^2} \sin^2\theta/\lambda^2)$, where $\overline{u_j^2}$ is the mean square atomic displacement in the x direction, modifies f_j strictly $f_{j,\theta}$, to take account of thermal vibration. Normally, $8\pi^2 \overline{u_j^2}$ is written as the isotropic temperature factor B_j, known as the Debye–Waller factor; initially in a structure determination, an overall value B, Sect. 4.2.1, may be applied to all atoms.

Thermal Vibration in Three Dimensions

We extend the discussion now to three dimensions, that is, to a lattice of scattering centers, or atoms, so as to obtain an expression analogous to (4.25). From (3.12), we derive an expression for the observed intensity I_o for a lattice of atoms at rest by multiplying this equation by its conjugate, which leads to:

$$I_\mathrm{o} = \Psi_{2\theta}^2 \sum_n \sum_m \exp\{\mathrm{i}2\pi[(\mathbf{r}_n - \mathbf{r}_m) \cdot \mathbf{S}]\} \tag{4.26}$$

where each summation extends over the total number of atoms in the unit cell. Small, vector displacements $\mathbf{u}_j$ are now applied to each atom, so that $\mathbf{r}_n$ is replaced by $\mathbf{r}_n + \mathbf{u}_n$, and similarly for $\mathbf{r}_m$, so that (4.26) becomes

$$I_\mathrm{o} = \Psi_{2\theta}^2 \sum_n \sum_m \exp\{\mathrm{i}2\pi[(\mathbf{r}_n - \mathbf{r}_m) \cdot \mathbf{S}]\} \times \exp\{\mathrm{i}2\pi[(\mathbf{u}_n - \mathbf{u}_m) \cdot \mathbf{S}]\} \tag{4.27}$$

The isotropic vibration of the lattice of atoms is expressed by the mean value of the second exponential term in (4.27). Let $2\pi[(\mathbf{u}_n - \mathbf{u}_m) \cdot \mathbf{S}]$ be written as $p_{n,m}$; then, for any particular value of $p_{n,m}$, we can write its mean value as

$$\overline{\exp(\mathrm{i}p)} = 1 + \overline{\mathrm{i}p} - \overline{p^2}/2! - \overline{\mathrm{i}p^3}/3! + \overline{p^4}/4! + \cdots = 1 - \overline{p^2}/2! + \overline{p^4}/4! \tag{4.28}$$

the mean values of the odd powers of p are zero, because positive and negative displacements are equally probable. A satisfactory approximation to (4.28) is then

$$\overline{\exp(\mathrm{i}p)} = \exp(-\overline{p^2}/2) \tag{4.29}$$

so that the mean value of (4.26) becomes

$$\bar{I}_\mathrm{o} = \Psi_{2\theta}^2 \sum_n \sum_m \exp\{\mathrm{i}2\pi[(\mathbf{r}_n - \mathbf{r}_m) \cdot \mathbf{S}]\} \exp(-\overline{p_{n,m}^2}/2) \tag{4.30}$$

Now $p_{n,m} = (4/\lambda)\ \pi \sin\theta(u_{n,S} - u_{m,S})$, where $u_{n,S}$ is the component of the nth displacement vector in the direction of the vector $\mathbf{S}$. Hence, we need to evaluate the mean value $\overline{(u_{n,S} - u_{m,S})^2}$, which is equivalent to $\overline{u_{n,S}^2} + \overline{u_{m,S}^2} - 2\overline{u_{n,S} u_{m,S}}$. We make the approximation that the coupling of the vibrations of atoms in a lattice is negligible, whereupon $\overline{u_{n,S} u_{m,S}} = 0$, and $\overline{u_{n,S}^2} = \overline{u_{n,S}^2} = \overline{u_S^2}$.

Table 4.1 Debye–Waller corrections for a carbon atom

			$\exp(-B^2\sin^2\theta/\lambda^2)$	
$\lambda^{-1}\sin\theta$	$(\lambda^{-1}\sin\theta)^2$	f	$B = 2$ Å^2	$B = 4$ Å^2
0	0	6	6	6
0.10	0.01	5.126	5.024	4.925
0.20	0.04	3.581	3.306	3.052
0.30	0.09	2.502	.090	1.746
0.40	0.16	1.950	1.416	1.028
0.50	0.25	1.685	1.022	0.620
0.60	0.36	1.536	0.748	0.364
0.70	0.49	1.426	0.535	0.201

In (4.26), the double summation contains N^2 terms. Those with $n = m$, a total of N, have an exponential factor of unity and $p_{n,m}$ is equal to zero. Where $n \neq m$, $\overline{p_{n,m}^2}/2$ is constant, because the vibration has been taken to be isotropic, and is equal to $2B$, where B is now given as

$$B = 8\pi^2\overline{u_S^2} \tag{4.31}$$

We can now write (4.27) as

$$I_o = \Psi_{2\theta}^2\left\{\sum_{\substack{n \\ n\neq m}}\sum_{m}\exp\{i2\pi[(\mathbf{r}_n - \mathbf{r}_m)\cdot\mathbf{S}]\}\exp[-2B(\sin^2\theta)/\lambda^2] + N\right\} \tag{4.32}$$

In the expression for the mean isotropic temperature factor B, $\overline{u_S^2}$ is the mean square atomic displacement in the direction of vector **S**, that is, normal to the reflecting plane to which $\sin\theta$ corresponds. Table 4.1 shows the effect of the exponential factor on the atomic scattering factor of carbon, for two values of B and from $\sin\theta/\lambda = 0 - 0.7$.

A better approximation for temperature correction assumes that the motion remains isotropic, but allows B to take a particular value B_j for each atom j in a unit cell of a structure. This procedure is used in the least-squares routine in the XRAY program, Sect. 13.4.4. In general, however, each atom in a structure vibrates anisotropically, and the time-averaged electron density for an atom has the form of a triaxial ellipsoid. This ellipsoid is represented by a 3×3 tensor, where six B_{ij} components are needed in the most general case of triclinic symmetry; the tensor is symmetric, that is, $B_{ij} = B_{ji}$. The B_{ij} values can be calculated from the isotropic B_j or B values, but normally are allowed to evolve in a least-squares refinement of atomic parameters.

Thermal vibrations increase the effective volume of the atom, so that interference within the atom becomes more noticeable. Consequently, f falls off with increasing $\sin\theta/\lambda$ more rapidly than with that calculated for an atom at rest, as shown in Fig. 4.6. The thermal vibrations of less rigidly retained atoms in a structure often have higher thermal vibrations than atoms that are more constrained by the stereochemistry. An example of this effect may be seen on the electron density map in Fig. 1.7: the carbon atoms in the eight-membered side chain have a greater freedom of movement than do those in the ring system; consequently, their thermal vibrations are larger and their electron density contours more diffuse.

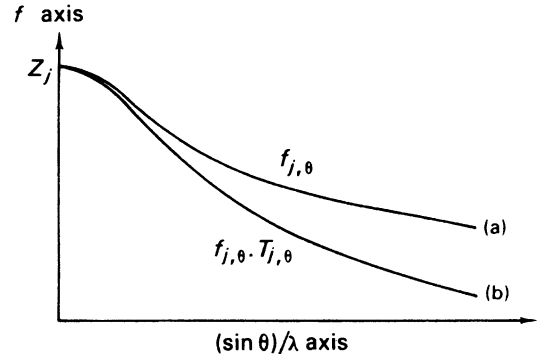

Fig. 4.6 Atomic scattering factors. (**a**) Stationary atom, $f_{j,\theta}$. (**b**) Atom corrected for thermal vibration, $f_{j,\theta}\ T_{j,\theta}$, also called $g_{j,\theta}$, where $T_{j,\theta} = \exp(-B^2 \sin^2\theta/\lambda^2)$.

Statistical Expectation Value of the Debye– Waller Factor

If the unit-cell distribution of the mean square displacement parameters of the atoms is assumed to be Gaussian, a *normal* distribution, with a mean $\bar{\mu}$ equal to $\bar{B}$, and a variance σ^2 equal to $(B - \bar{B})^2$, then the expectation value $\overline{W^2}$ for the Debye–Waller factor is given as $\overline{W^2} = \exp[-2(\overline{\mu} - \sigma^2 s^2)^2]$, where $W^2 = \exp(-2Bs^2)^2$ and $s = \sin\theta/\lambda$. This result has been incorporated into procedures for scaling and normalizing measured intensities to the Wilson expectation values. The procedures can be used to determine both isotropic $\overline{\mu_B}$ and σ_B, and anisotropic $\overline{\mu}_{U_{ij}}$ and $\sigma_{U_{ij}}$ distribution parameters. Tests with experimental data and refined structural models for several protein crystals have yielded reliable normalized structure factors, Sect. 4.2.5, with $\Sigma_{\mathbf{h}}|E - |E_c||/\Sigma_{\mathbf{h}}E \approx 5\%$.

4.2 Intensity Statistics

Statistics form an important adjunct to many aspects of X-ray crystallography. They are used in assessing the precision of unit-cell and atomic parameters, for predicting the phase angles of reflections by direct methods, as discussed in Chap. 8, for determining scale and temperature factors, to name but three. In this section, we shall be concerned with the statistics of intensity distributions, and we consider first the Wilson statistics, and show how they may be used to obtain scale and temperature factors for a crystal.

4.2.1 Determining Scale and Temperature Factors

Wilson Plot

An important and familiar aspect of the statistics of the weighted reciprocal lattice is based on the equation developed by Wilson [6] for the average ideal intensity. We write (3.63), for convenience, in a compact form:

$$F(\mathbf{h}) = \sum_j g_{j,\theta} \exp[i2\pi(\mathbf{h} \cdot \mathbf{r}_j)] \tag{4.33}$$

where **h** represents the reciprocal lattice point *hkl*, $\mathbf{r}_j$ is the position vector of the *j*th atom, that is, $\mathbf{r}_j = x_j\mathbf{a} + y_j\mathbf{b} + z_j\mathbf{c}$; $g_{j,\theta}$ is the atomic scattering factor for the *j*th atom, f_j, modified by a temperature factor, such as $\exp(-B^2\sin^2\theta/\lambda^2)$, and the sum is over all atoms in the unit cell.

If we now multiply (4.33) by its conjugate, we obtain an expression for the ideal intensity $|\mathrm{F}(\mathbf{h})|^2$:

$$|\mathrm{F}(h)|^2 = \sum_j g_{j,\theta}^2 + \sum_{\substack{j \\ j\neq k}} \sum_k g_{j,\theta} g_{k,\theta} \exp(\mathrm{i}2\pi\mathbf{h}\cdot\mathbf{r}_{j,k}) \tag{4.34}$$

where $\mathbf{r}_{j,k}$ is the vector distance $\mathbf{r}_j - \mathbf{r}_k$. If the distribution of atoms is uniform over the unit cell, then the second term on the right-hand side of (4.34) will tend to a negligible value because the many $\mathbf{r}_{j,k}$ vectors will tend to cancel one another: then, the average ideal intensity is given by

$$\overline{|\mathrm{F}(\mathbf{h})|^2} = \sum_j g_{j,\theta}^2 \tag{4.35}$$

and is the basis for obtaining a preliminary scale factor for F_o and a temperature factor for *f*.

Equation (4.35) has been found to hold satisfactorily over a wide range of structures, provided that the values of F_o^2 are averaged over small, local ranges *r* in reciprocal space, such that *f* is not varying rapidly within any range.

Applying the scale and temperature factors to (4.35), we have

$$K^2\overline{F_\mathrm{o}(\mathbf{h})^2} = \exp(-2B\sin^2\theta_r/\lambda^2) \sum_j f_{j,\theta_r}^2 \tag{4.36}$$

where θ_r is a representative value of θ for each range and f_{j,θ_r} the corresponding rest-atomic scattering factor. Taking logarithms of both sides, we write

$$\ln q_r = 2\ \ln\ K + 2B\sin^2\theta_r/\lambda^2 \tag{4.37}$$

where q_r is given by

$$q_r = \left(\sum_j f_{j,\theta_r}^2\right) \Big/ \overline{F_\mathrm{o}(\mathbf{h})_{\theta,r}^2} \tag{4.38}$$

and the sum is taken over all *j* atoms in the unit cell. If $\ln\ q_r$ is plotted against $\sin^2\theta_r/\lambda^2$ and the best straight line drawn, the slope is equal to $2B$ and the intercept on the ordinate is equal to $2\ \ln\ K$. This graph is often called a Wilson plot and is best obtained through the following procedure.

Methodology

1. Three-dimensional space is divided into a number of spherical shells, Fig. 4.7a, such that there are 80–100 reflections in each range. Although the plot of Fig. 4.7b is against $\sin^2\theta/\lambda^2$, it is convenient to form the range demarcations in terms of $\sin^3\theta/\lambda^3$, since this parameter has the dimensions of reciprocal volume; the demarcations can be converted into the equivalent values of $\sin^2\theta/\lambda^2$ later.
2. Average values of $F_\mathrm{o}(\mathbf{h})^2$ for each range are calculated, including either symmetry-equivalent reflections, or according each reflection in the asymmetric unit its correct multiplicity of planes. It is necessary also to allocate values to the accidental absences, that is, possible reflections lying within the experimental Ewald sphere that are too weak to be recorded.

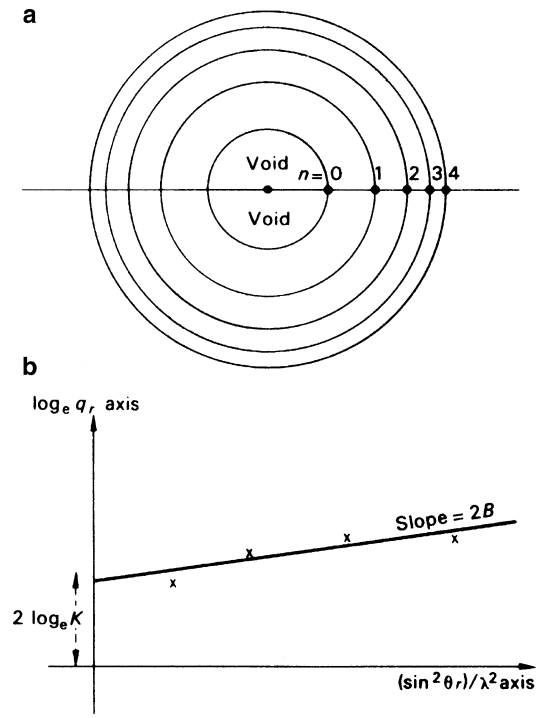

Fig. 4.7 Scale and temperature factors. (**a**) Division of reciprocal space into spherical shells; the void region contains data for which $h, k, l < 2$. (**b**) Wilson plot: the intercept is 2 ln K, and the slope is $2B$

Wilson [6] has shown that the most probable values for accidental absences are $0.55F_{\mathrm{o,min}}$ for centrosymmetric crystals, $0.66F_{\mathrm{o,min}}$ for non-centrosymmetric crystals, and $0.59F_{\mathrm{o,min}}$ where this symmetry is undetermined; $F_{\mathrm{o,min}}$ is the minimum value of $F_{\mathrm{o}}(\mathbf{h})$ in the range under consideration. Systematic absences are always ignored, as are those in a region up to the second order on each axis because they are atypical of the general distribution of intensities. In addition, the *average intensity multiple* (ε-factor) should be applied as a divisor of each intensity value; this parameter is discussed and tabulated in Sect. 4.2.3.

3. The mean values of $\sin^2\theta_r/\lambda^2$ may be obtained as

$$\sin^2\theta_r/\lambda^2 = \frac{1}{2}(\sin^2\theta_n/\lambda^2 + \sin^2\theta_{n+1}/\lambda^2)$$

where $n + 1$ is the number of the outer boundary shell defining the rth shell, starting at $n = 0$ for which value $\sin\theta = \sin\theta_{\min}$, Fig. 4.7a. Alternatively, $\sin^2\theta_r/\lambda^2$ values may be obtained as averages of $\sin^2\theta/\lambda^2$ over each range. Atomic scattering factor data are tabulated and readily available [7].

Auxiliary Plot

The Wilson plot can sometimes be non-linear, possibly because (4.35) does not hold well for the given data. It may be useful to make an auxiliary plot in which the numerator in (4.38) is replaced by $\sum_j Z_j^2$, that is, the sum of the squares of f_j at $\theta = 0$. Both curves should have the same intercept, and experience indicates that a compromise between the Wilson and auxiliary plots often leads to a better result.

4.2.2 Other Aspects of the Wilson Plot

In papers dealing with the calculation of |E| values, Hall and Subramanian consider the Wilson plot in some detail [8]. They stress the need for the shells in the Wilson plot to be equally populated, which means that F_o values for the accidentally absent reflections should be estimated with care. The program GENEV [9] provides two methods for calculating |E| values: one uses the values of B and K from the linear Wilson plot, whereas the other provides inter alia the options of linear scale, profile scale, and random fragment; the program GENEV uses Bayesian statistics [10] to obtain reliable estimates of weak reflections.

Pathological Cases

Assuming that all possible care has been taken in collecting the intensity data, there may still remain some situations in which the Wilson plot is non-linear, for a variety of reasons: there may be significant non-zero values of the double summation in (4.34) or the temperature factor is non-Gaussian, both conditions leading to a partial breakdown of (4.35), on which equation the Wilson plot is based. Alternatively, the number of atoms in the unit cell may be too low to provide a uniform distribution; a proportion of atoms may lie on symmetry elements, and so contribute only to certain reflections; the proportion of heavy atoms in the unit cell may be unduly large; hypersymmetry may be present. Some of these problems have been addressed by several workers, but no totally satisfactory procedure has emerged. In most cases, the problem is resolved in the least-squares refinement of the structure; hypersymmetry is discussed briefly in Sect. 4.2.5.

In handling two-dimensional data, the annular regions of equal area may contain too few reflections for a true sample of the reciprocal lattice. Then it is possible to employ a batch procedure, that is, to combine groups (1, 2), (2, 3), (3, 4),. . . before the averages are taken.

In the program XRAY, the routine for the Wilson plot uses this batch technique for the two-dimensional data sets. Not all of the example data sets provided give equally satisfactory results; this situation is considered again in Sect. 4.2.5.

4.2.3 Statistics of Reciprocal Space

The weighted reciprocal lattice exhibits four types of regularity and one type that may be described as irregular; we shall consider them in turn.

Accidental Absences

Accidental absences occur in the diffraction pattern of most structures, and they are disposed in an *irregular* manner within the Ewald sphere. From (3.63), it is not surprising to find that there are some instances where the sum of the vectors $f_j \exp[i2\pi(hx_j + ky_j + lz_j)]$ tend to cancel to a negligible value. The result depends upon the particular atomic arrangement in the structure rather than on its symmetry. Such permitted reflections of negligible intensity can be estimated in the manner discussed in Sect. 4.2.1: it is not uncommon to omit these reflections from a structure analysis, but without real justification. We now consider *regular* features of the weighted reciprocal lattice.

Laue Symmetry

The positions of the reciprocal lattice points and the intensities associated with them conform to one of the Laue groups, that is, one of the eleven centrosymmetric point groups discussed in Sect. 1.4.2. This situation arises because of Friedel's Law, Sect. 3.6.1, and holds in all normal situations, that is, in the absence of resonance excitation, Sect. 3.1.3.

Systematic Absences

In the presence of translational symmetry, that is, structures with centered unit cells, glide planes, or screw axes, certain characteristic groups of reflections are absent from the diffraction records, Sect. 3.7ff. The diffracted energy that is so excluded is redistributed over other reflections. For example in a *C*-centered unit cell, *hkl* reflections are absent for $h + k = 2n + 1$. However, the structure factor equation now takes the form

$$\mathrm{F}(hkl) = 2[\cos^2\pi(h+k)/4]\sum_{j=1}^{n} g_j \times \exp[\mathrm{i}2\pi(hx_j + ky_j + lz_j)] \tag{4.39}$$

from which it is evident that for the reflections present, $(h + k)$ even, $|\mathrm{F}(hkl)|$ has twice the value that it would have for a corresponding primitive unit cell.

Abnormal Averages

We have shown in Sect. 3.2.3 that the components of (4.33) can be represented in phase and amplitude on an Argand diagram. All types of symmetry link the $\mathbf{r}_j$ ($\mathbf{r}_j = x_j\mathbf{a} + y_j\mathbf{b} + z_j\mathbf{c}$) in groups of two or more; (3.69) represents the simplest example of this feature. Thus, $\sum_j g_j^2$, which we shall write as Σ, is enhanced and becomes a *distribution parameter* S (not to be confused with $S = 2\sin\theta/\lambda$):

$$S = \varepsilon\Sigma = \varepsilon\sum_{j=1}^{n} g_j^2 \tag{4.40}$$

Consider space group *Pm*, where the mirror plane is normal to y and cuts this axis at $y = 0$; then, atoms are related in pairs x, y, z, and $x, \bar{y}, z$. Simple manipulation shows that the structure factor equation for this example becomes

$$\mathrm{F}(hkl) = \sum_{j=1}^{n/2} g_j \exp[\mathrm{i}2\pi(hx_j + ky_j)](2\cos 2\pi lz_j) = A'(hkl) + \mathrm{i}B'(hkl) \tag{4.41}$$

where

$$A'(hkl) = 2\sum_{j=1}^{n/2} g_j \cos 2\pi(hx_j + lz_j)\cos 2\pi ky_j \tag{4.42}$$

and

$$B'(hkl) = 2\sum_{j=1}^{n/2} g_j \sin 2\pi(hx_j + lz_j)\cos 2\pi ky_j \tag{4.43}$$

We need now to invoke the *central limit theorem* which states that *in a sequence of independent random variables* $x_1, x_2, \ldots, x_j, \ldots, x_n$, *where the mean values are expressed by* m_j *and the variances by* σ_j^2, *the sum* $x = \Sigma_j x_j$ *tends to a normal* (*Gaussian*) *distribution*, *with a mean m equal to* $\Sigma_j m_j$ *and a variance* σ^2 *equal to* $\Sigma_j\sigma_j^2$, *as the number of terms* (*n*) *in the sequence tends*, *ideally*, *to infinity*.

In our application, the mean values $\overline{A'(hkl)}$ and $\overline{B'(hkl)}$ both tend to zero, since the positive and negative values of these terms are equally probable and will tend to cancel one another in a normal distribution. The variance for a large sample is given generally by

$$\sigma^2 = (1/n)\sum_j (x_j - \bar{x})^2 = (1/n)\sum_j x_j^2 - \overline{x^2} \tag{4.44}$$

since $\bar{x} = 0$ in our example, $\sigma^2 = \overline{x_j^2}$. Applying this result first to $A'(hkl)$, the jth individual variance is given by $2g_j^2\cos^2 2\pi(hx_j + lz_j)\cos^2\ 2\pi(ky_j)$. Thus, the variance of $A'(hkl)$ will be equal to $\overline{A'(hkl)^2}$ which, by the central limit theorem, is given by

$$\begin{aligned}\overline{A'(hkl)^2} &= \sum_{j=1}^{n/2} 4g_j^2\overline{\cos^2 2\pi(hx_j + lz_j)\cos^2 2\pi ky_j} \\ &= \sum_{j=1}^{n/2} 4g_j^2\overline{\cos^2 2\pi(hx_j + lz_j)}\ \overline{\cos^2 2\pi ky_j}\end{aligned} \tag{4.45}$$

It is straightforward to show, since $\overline{\cos^2\theta} = (1/\pi)\int_0^\pi \cos^2\theta\ \mathrm{d}\theta$, that the average value of $\cos^2\ \theta$ is $\frac{1}{2}$. Hence, from (4.40),

$$\overline{A'(hkl)^2} = \sum_{j=1}^{n/2} g_j^2 = \frac{1}{2}\Sigma \tag{4.46}$$

In a similar manner, we can show that the average $\overline{B'(hkl)^2}$ is also equal to $\frac{1}{2}\Sigma$,so that

$$\overline{|\mathrm{F}(hkl)^2|} = \Sigma \tag{4.47}$$

However, if we consider the zone of reflections for which $k = 0$, a similar analysis shows that

$$\overline{|\mathrm{F}(h0l)^2|} = 2\Sigma \tag{4.48}$$

Hence, the ε-factor for the *intensities* in this zone of $P2/m$ is 2. The ε-factor is dependent on the *crystal class*, and Table 4.2 lists the ε-factors that arise in the 32 point groups.

Another way of looking at these ε-factors is by means of stereograms. Consider Fig. 1.31, point group $\bar{4}2m$, and imagine the radiating normals that give rise to the poles as vectors. When *projected* onto the z axis there is a fourfold *superposition* of the g_j vectors, but when projected onto the plane normal to z there is no such superposition; hence, 4/1 arises for the first direction, along z, that is, $\varepsilon(00l) = 4$ and $\varepsilon(hk0) = 1$.

4.2.4 Acentric and Centric Distributions of Structure Factors

The measured intensities of the whole reciprocal lattice or of certain two- or even one-dimensional regions of it may conform to an *acentric*,[2] a *centric*, or a *hypercentric* distribution, and we shall consider the properties and uses of their distribution functions.

[2] Not "non-centrosymmetric" and "centrosymmetric."

Table 4.2 Centric reflections and multiples (ε-factors) for intensities in the 32 crystal classes

Crystal class	New diffraction symbol	Centric sets	Multiples
1	1*P*	None	1/1
$\bar{1}$	$\bar{1}\underline{P}$	All	1/1
m	2/*mP*–/–	(0*k*0)	1/2
2	2/*mP*–/$\underline{\ }$	(*h*0*l*)	2/1
2/*m*	2/*m*$\underline{P}$–/–	All	2/2
*mm*2	*mmmP*– – $\underline{\ }$	[(*hk*0) masks (*h*00), (0*k*0)]	2/2; 2/2; 4/1
222	*mmmP*–$\underline{\ }$ $\underline{\ }$ $\underline{\ }$	3 principal zones only	2/1; 2/1; 2/1
mmm	*mmm*$\underline{P}$– – –	All	4/2; 4/2; 4/2
4	4/*mP*–/$\underline{\ }$	(*hk*0)	4/1
$\bar{4}$	4/*mP*–/$\underline{\ }$	(*hk*0); (00*l*)	2/1
4/*m*	4/*m*$\underline{P}$–/–	All	4/2
$\bar{4}$2*m*	4/*mmmP*–/$\underline{\ }$ $\underline{\ }$ –	[(*hk*0), {*hh*0}]; [{*h*0*l*}, (00*l*)]	4/1; 2/1; 2/2
4*mm*	4/*mmmP*–/$\underline{\ }$ – –	[(*hk*0), {*h*00}, {*hh*0}]	8/1; 2/2; 2/2
422	4/*mmmP*–/$\underline{\ }$$\underline{\ }$ $\underline{\ }$	(*hk*0); {*h*0*l*}; {*hhl*}	4/2; 2/1; 2/1
4/*mmm*	4/*mmm*$\underline{P}$–/– – –	All	8/2; 4/2; 4/2
3	$\bar{3}P$–	None	3/1
$\bar{3}$	$\bar{3}\underline{P}$–	All	3/1
3*m*(1)	$\bar{3}$*mlP*– – –	{*h*0$\bar{h}$0}	6/1; 1/2; 2/1
32(1)	$\bar{3}$*mlP*– $\underline{\ }$ –	{*h*0$\bar{h}$*l*}	3/1; 2/1; 1/1
$\bar{3}$*m*(1)	$\bar{3}$*ml*$\underline{P}$– – –	All	6/1; 2/2; 2/1
$\bar{6}$	6/*mP*–/$\underline{\ }$	(*hk*0)	6/1
$\bar{6}$	6/*mP*–/–	(00*l*)	3/2
6/*m*	6/*m*$\underline{P}$–/–	All	6/2
$\bar{6}$*m*2	6/*mmmP*–/– – $\underline{\ }$	[{*hhl*}, {*hh*0}, (00*l*)]	6/2; 2/2; 4/1
6*mm*	6/*mmmP*–/$\underline{\ }$ – –	[(*hk*0), {*hh*0}, {*h*00}]	12/1; 2/2; 2/2
622	6/*mmmP*–/$\underline{\ }$$\underline{\ }$ $\underline{\ }$	(*hk*0); (*h*0*l*); (*hhl*)	6/1; 2/1; 2/1
6/*mmm*	6/*mmm*$\underline{P}$–/– – –	All	12/2; 4/2; 4/2
23	*m*3*P*$\underline{\ }$ –	{*hk*0}	2/1; 3/1; 1/1
m$\bar{3}$	*m*3$\underline{P}$– –	All	4/2; 3/1; 2/1
$\bar{4}$3*m*	*m*3*mP*$\underline{\ }$ – –	[{*hk*0}, {*hh*0}]	4/1; 6/1; 2/2
432	*m*3*mP*$\underline{\ }$ – $\underline{\ }$	{*hk*0}; {*hhl*}	4/1; 3/1; 2/1
m$\bar{3}$*m*	*m*3*m*$\underline{P}$– – –	All	8/2; 6/1; 4/2

Column 1: Crystal class (also point group symbol)
Column 2: Buerger diffraction symbols: centric zones are underlined, and the unit cell symbol is underlined where the point group is centrosymmetric. Note that the centric distribution occurs (i) for all *hkl* if the lattice is centrosymmetric; (ii) for a zone if the corresponding projection is centrosymmetric; (iii) for a central lattice row if the corresponding one-dimensional projection is centrosymmetric
Column 3: Centric reflections are listed explicitly
Column 4: Average intensity crystal class-dependent multiples (ε-factors). Each *p*/*q* symbol gives the multiple *p* (ε-factor) for a reciprocal lattice row and *q* that for the zone normal to the row
Column 5. It may be helpful to recall the full symbols 1*m*1, 121 (monoclinic *m* and 2).

Acentric Distribution

In the acentric distribution, typically for space group *P*1, the components $A'(\mathbf{h})$ and $B'(\mathbf{h})$ of the structure factor must be considered separately. Following earlier discussions we write $A'(\mathbf{h})$, omitting the subscript θ to g, as

$$A'(\mathbf{h}) = \sum_{j=1}^{n} g_j \cos 2\pi(\mathbf{h} \cdot \mathbf{r}_j)$$

and its average value over j atoms is zero, as discussed above; then from (4.46)

$$\overline{A'(\mathbf{h})^2} = \sum_{j=1}^{n} g_j^2 \overline{\cos^2 2\pi(\mathbf{h} \cdot \mathbf{r}_j)} = \frac{1}{2}\Sigma \tag{4.49}$$

Similarly, $\overline{B'(\mathbf{h})} = 0$, and $\overline{B'(\mathbf{h})^2} = \frac{1}{2}\Sigma$. The probabilities that A' lies between A' and $A' + \mathrm{d}A'$, and that B' lies between B' and $B' + \mathrm{d}B'$, following a normal distribution of the type $P(x) = (2\pi\sigma^2)^{-1/2} \exp[-(x - \bar{x})^2/2\sigma^2]$, are

$$\begin{aligned} P_\mathrm{a}(A')\,\mathrm{d}A' &= 1/(\pi\Sigma)^{1/2} \exp(-A'^2/\Sigma)\,\mathrm{d}A' \\ P_\mathrm{a}(B')\,\mathrm{d}B' &= 1/(\pi\Sigma)^{1/2} \exp(-B'^2/\Sigma)\,\mathrm{d}B' \end{aligned} \tag{4.50}$$

The region of area defined by $\mathrm{d}A'\ \mathrm{d}B'$ is an infinitesimal portion of an annular ring on an Argand diagram, Fig. 4.8, distant $|\mathrm{F}|$ from the origin. Since A' and B' are not correlated, the joint probability that the structure amplitude $|\mathrm{F}|$ lies between $|\mathrm{F}|$ and $|\mathrm{F}| + \mathrm{d}|\mathrm{F}|$ is

$$\begin{aligned} P_\mathrm{a}(|\mathrm{F}|)\,\mathrm{d}|\mathrm{F}| = P_\mathrm{a}(A')P_\mathrm{a}(B')\,\mathrm{d}A'\,\mathrm{d}B' &= (1/\pi\Sigma) \exp[-(A'^2 + B'^2)/\Sigma]\,\mathrm{d}A'\,\mathrm{d}B' \\ &= (1/\pi\Sigma) \exp[(-|\mathrm{F}|^2)/\Sigma]\,\mathrm{d}|S| \end{aligned} \tag{4.51}$$

where $\mathrm{d}|S|$ represents an area $\mathrm{d}A'\ \mathrm{d}B'$ on the Argand diagram and has the value $2\pi|\mathrm{F}|\ \mathrm{d}|\mathrm{F}|$. Thus, the joint probability refers to that area of the annular ring on the Argand diagram with radii $|\mathrm{F}|$ and $|\mathrm{F}| + \mathrm{d}|\mathrm{F}|$, so that the acentric distribution function is

$$P_\mathrm{a}(|\mathrm{F}|) = (2|\mathrm{F}|/\Sigma) \exp[(-|\mathrm{F}|^2)/\Sigma] \tag{4.52}$$

Centric Distribution

Space group $P\bar{1}$ provides a typical centric distribution of intensity data. The structure factors are real and are given by the A' component of the structure factor equation, that is,

$$F(\mathbf{h}) = A'(\mathbf{h}) = 2\sum_{j=1}^{n/2} g_j \cos 2\pi(\mathbf{h} \cdot \mathbf{r}_j) \tag{4.53}$$

where $\mathbf{h}$ and $\mathbf{r}_j$ have the meanings as before. From the central limit theorem, if the set of $A'(\mathbf{h})$ follows a normal distribution, the mean $\overline{A'(\mathbf{h})}$ is zero, and the variance $\overline{A'(\mathbf{h})^2}$ is the sum of $n/2$ terms of the form $4g_j^2\ \overline{\cos^2 2\pi(\mathbf{h} \cdot \mathbf{r}_j)}$, which evaluates to Σ, the distribution parameter defined above. Hence, the probability that a structure factor lies between F and $F + \mathrm{d}F$ is given by

$$P_\mathrm{c}(F)\,\mathrm{d}F = 1/(2\pi\Sigma)^{1/2} \exp(-F^2/2\Sigma)\,\mathrm{d}F \tag{4.54}$$

and the centric distribution function becomes

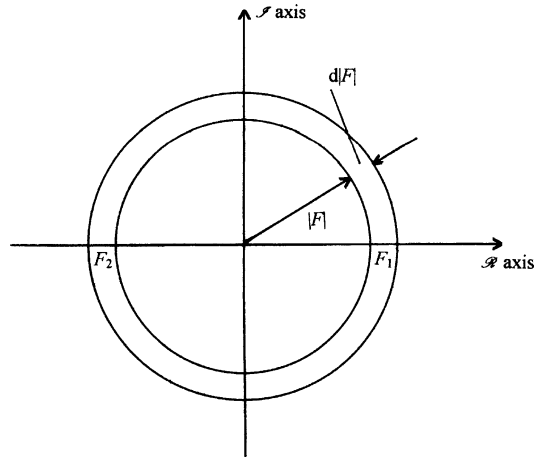

Fig. 4.8 Region on an Argand diagram for structure amplitude lying between |F| and |F| + d|F| in an acentric distribution. In a centric distribution, F can have only two possible values, shown at F_1 (+|F|) and F_2 (−|F|)

$$P_c(F) = (2\pi\Sigma)^{-1/2} \exp(-F^2/2\Sigma) \tag{4.55}$$

We note that, if we wish to consider here only the *amplitudes* of the centric structure factors, a phase-restricted set, then it follows that

$$P_c(F_{amp}) = 2P_c(F) = (2/\pi\Sigma)^{1/2} \exp(-F^2/2\Sigma) \tag{4.56}$$

since the amplitude of F can be derived from either (+)F or (−)F, Fig. 4.8. We use this function in deriving $N_c(E)$ shortly, because we will be concerned only with positive values in the centric distribution of amplitudes.

Mean Values

We are now in a position to derive mean values for |F| and $|F|^2$ and other parameters in the two distributions derived. The mean value $\bar{x}$ for any distribution $\phi(x)$ is given generally by

$$\bar{x} = \frac{\int x\phi(x)\,dx}{\int \phi(x)\,dx}$$

but, because we are dealing with a normal distribution, $\int \phi(x)\,dx = 1$, so that the average value of x is given simply by

$$\bar{x} = \int x\phi(x)\,dx \tag{4.57}$$

The acentric and centric intensity distributions are plotted in terms of |F| in Fig. 4.9. It is evident that the centric distribution is characterized by a significant proportion of both strong and weak intensities, whereas the acentric distribution has a low dispersion of intensities. These features can sometimes be recognized in precession X-ray photographs, Sect. 5.4ff.

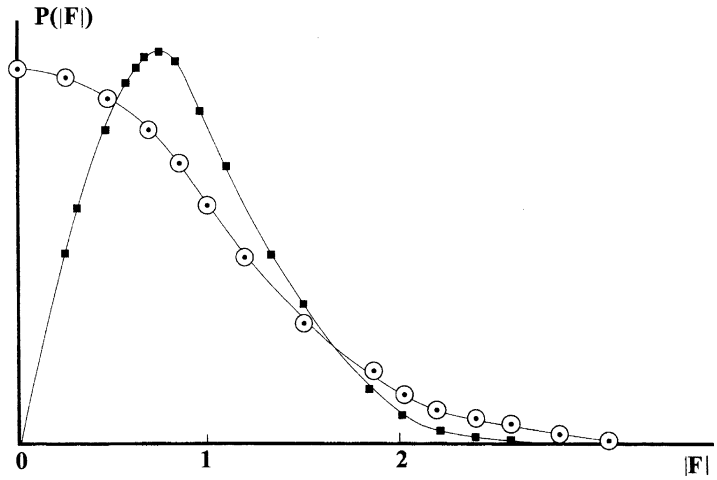

Fig. 4.9 Distribution function for structure amplitudes: (**a**) acentric, ■ (**b**) centric ⊙. The acentric distribution has a low dispersion of |F| values, whereas the centric distribution has significant proportions of both small and large |F| values

Because the centric and acentric distributions differ, it is reasonable to suppose that the distributions may be used to distinguish between centrosymmetric and non-centrosymmetric crystals. We have noted in Sect. 3.8 that the space group suggested by the diffraction data of a crystal may often be ambiguous. The cause of the ambiguity lies frequently in Friedel's law, that is, the inability to determine from the positions of the diffraction spectra alone whether or not the crystal itself is centrosymmetric.

A parameter that may be used as a discriminator is the ratio of the square of the average |F| to the average of $|F|^2$:

$$M = |\overline{F}|^2 / \overline{|F|^2} \tag{4.58}$$

For the acentric distribution, we have

$$\overline{|F|} = (2/\Sigma) \int_0^\infty |F|^2 \exp(-|F|^2/\Sigma) \mathrm{d}|F|$$

This integral, and many similar to it, can be solved readily by making use of the properties of the gamma (Γ) function (see Web Appendix WA7). Let $|F|^2/\Sigma = t$, so that $2|F|\ \mathrm{d}|F| = \Sigma\ \mathrm{d}t$. Then,

$$\overline{|F|} = \Sigma^{1/2} \int_0^\infty t^{1/2} \exp(-t)\ \mathrm{d}t$$

The term $t^{1/2}$ may be written as $t^{(3/2-1)}$, so that the value of the integral is $\Gamma(3/2)$ or $\frac{1}{2}\pi^{1/2}$, so that

$$\overline{|F|} = \frac{1}{2}(\pi\Sigma)^{1/2} \tag{4.59}$$

In a similar manner,

$$\overline{|F|^2} = (2/\Sigma) \int_0^\infty |F|^3 \exp(-|F|^2/\Sigma)\, \mathrm{d}|F| \tag{4.60}$$

By making substitutions as before, it is straightforward to show that the integral in (4.60) equates to Σ. Thus,

$$M_a = \frac{1}{4}\pi\Sigma/\Sigma = \pi/4 = 0.785 \tag{4.61}$$

In a centric distribution, the corresponding parameter M_c is readily shown to be

$$M_c = (2\Sigma/\pi)/\Sigma = 2/\pi = 0.637 \tag{4.62}$$

A disadvantage inherent in these discriminators, even when the data are divided into ranges in which the variation of f (or g) with θ is small, is that the variation is imposed on the results. It is preferable, therefore, to use a parameter that is not dependent upon f.

4.2.5 Normalized Structure Factors

In the previous section, we stressed the importance of placing intensity data on a common statistical scale, and we discussed the ε-factor for the crystal classes. For improved statistical results, either *unitary* structure factors U(**h**) or *normalized* structure factors E(**h**) are employed: $|U(\mathbf{h})|^2 = |E(\mathbf{h})|^2 \Sigma_j g_j^2/(\Sigma_j g_j)^2$. We shall use the parameter |E| in discussing intensity statistics and direct methods.

The normalized structure factor E is given by the equation

$$|E|^2 = |F|^2 \Big/ \varepsilon \sum_j g_j^2 \tag{4.63}$$

where |F| is on an absolute scale. For special classes of reflections, the ε-factor must be applied in accordance with Table 3.10.

From (4.52), the acentric distribution function for normalized structure factors follows as

$$P_a(|E|) = 2|E| \exp(-|E|^2) \tag{4.64}$$

and from (4.55), that for the centric distribution is

$$P_c(E) = (2\pi)^{-1/2} \exp(-E^2/2) \tag{4.65}$$

Again, as with the centric distribution of |F|, the distribution of |E| amplitudes in the centric case is twice that given in (4.65), because |E| here includes both $+E$ and $-E$:

$$P_c(|E|) = (2/\pi)^{1/2} \exp(-|E|^2/2) \tag{4.66}$$

It will be evident that these distribution equations do not involve the atomic scattering factors, so they are independent of the particular structure. As in the previous section, we can calculate mean values related to the new variable |E|. For both the acentric and the centric distributions, the average value of $|E|^2$ is unity. For the average value of |E| in the acentric distribution, we have

Table 4.3 Parameters in the acentric and centric distributions of |E| values

Parameter	Acentric	Centric
$\overline{\lvert E \rvert}$	0.886	0.798
$\overline{\lvert E \rvert^2}$	1	1
$\overline{\lvert E \rvert^2 - 1}$	0.736	0.968
$\overline{(\lvert E \rvert^2 - 1)^2}$	1	2

$$\overline{|\mathrm{E}|} = 2\int_0^\infty |\mathrm{E}|^2 \exp(-|\mathrm{E}|^2)\, \mathrm{d}|\mathrm{E}|$$

Making the substitution $|\mathrm{E}|^2 = t$, the integral becomes

$$\overline{|\mathrm{E}|} = \int_0^\infty t^{1/2} \exp(-t)\, \mathrm{d}t$$

Since $t^{1/2}$ may be written as $t^{3/2-1}$, the integral becomes $\Gamma(3/2)$, or $\frac{1}{2}\Gamma(1/2)$, which is $\frac{1}{2}\sqrt{\pi}$. Hence, $\overline{|\mathrm{E}|} = 0.886$. In the case of the centric distribution, a similar calculation shows that $\overline{|\mathrm{E}|} = 0.798$.

The parameter $|\mathrm{E}|^2 - 1|$ offers another useful discriminant between acentric and centric distributions. Here, we evaluate this parameter for the centric distribution; that for the acentric distribution forms a problem at the end of the chapter. We now use $\overline{|\mathrm{E}^2 - 1|}$ for the centric case—$(+\mathrm{E})^2 = (-\mathrm{E})^2$:

$$\begin{aligned}\overline{|\mathrm{E}^2 - 1|} &= (2/\pi)^{1/2} \int_0^\infty \overline{|\mathrm{E}|^2 - 1|} \exp(-\mathrm{E}^2/2)\, \mathrm{dE} \\ &= (2/\pi)^{1/2} \int_0^1 (1 - \mathrm{E}^2) \exp(-\mathrm{E}^2/2)\, \mathrm{dE} + (2/\pi)^{1/2} \int_1^\infty (\mathrm{E}^2 - 1) \exp(-\mathrm{E}^2/2)\, \mathrm{dE}\end{aligned}$$

Since, generally,

$$\int (1 - X^2) \exp(-X^2/2)\, \mathrm{d}X = \int \mathrm{d}[X \exp(-X^2/2)] \tag{4.67}$$

it follows that

$$\begin{aligned}\overline{|\mathrm{E}^2 - 1|} &= (2/\pi)^{1/2} \left\{ \int_0^1 \mathrm{d}[\mathrm{E} \exp(-\mathrm{E}^2/2)] + \int_\infty^1 \mathrm{d}[\mathrm{E} \exp(-\mathrm{E}^2/2)] \right\} \\ &= (2/\pi)^{1/2} \{ \mathrm{E} \exp(-\mathrm{E}^2/2)|_0^1 + \mathrm{E} \exp(-\mathrm{E}^2/2)|_\infty^1 \} \\ &= (2/\pi)^{1/2} 2\mathrm{e}^{-1/2} = 0.968\end{aligned}$$

A range of parameters can be determined from the probability functions for the two distributions; a few of them are listed in Table 4.3.

The centric distribution is addressed again through Problems 4.3 and 4.5.

Table 4.4 Acentric and centric cumulative distributions

$\|E\|$	$N_a(\|E\|)$	$N_c(\|E\|)$
0	0	0
0.2	0.039	0.159
0.4	0.148	0.311
0.6	0.302	0.451
0.8	0.473	0.576
1.0	0.632	0.683
1.2	0.763	0.770
1.4	0.859	0.838
1.6	0.923	0.890
1.8	0.961	0.928
2.0	0.982	0.954
2.2	0.992	0.972
2.4	0.997	0.984
2.6	0.999	0.991
2.8	1.000	0.995
3.0	1.000	0.997

Cumulative Distributions

Rather than considering individual parameters, such as M or $\overline{|E|}$, the determination of the centricity or otherwise of the distribution may be approached by means of cumulative distributions of $|E|$ values. In the acentric distribution, the fractional number of $|E|$ values less than or equal to a given value of $|E|$ is the integral of the probability function from the lower limit to that given value. Thus, we write for the acentric distribution

$$N_a(|E|) = 2\int_0^{|E|} |E| \exp(-|E|^2)\, d|E| = 1 - \exp(-E^2) \tag{4.68}$$

Similarly, for the centric distribution, we have

$$\begin{aligned} N_a(|E|) &= 2\int_0^{|E|} |E| \exp(-|E|^2)\, d|E| \\ &= \text{erf}\ (|E|/\sqrt{2}) \end{aligned} \tag{4.69}$$

where erf(...) represents the statistical error function, which is tabulated in most texts on statistics. Table 4.4 list the values of $N(|E|)$ for the two distributions up to $|E| = 3.0$, and Fig. 4.10 illustrates these distributions; the region of greatest discrimination is clearly $0<|E|<1$.

Hypersymmetry

Hypersymmetry (hyper-centrosymmetry) can arise when non-crystallographic centers of symmetry are present in the asymmetric unit of a structure. Pyrene [11] and benzo[*a*]pyrene [12] are examples of molecules that are, themselves, centrosymmetric; the crystal structure of pyrene has been reported in space group $P2_1/a$, which is a non-standard setting of $P2_1/c$. The degree of hypersymmetry depends upon the number of additional centers of symmetry. Figure 4.10 includes the curve for $N_h(|E|)$ when one additional center is present in the asymmetric unit. Further discussions on hypersymmetry may be found in the literature [13].

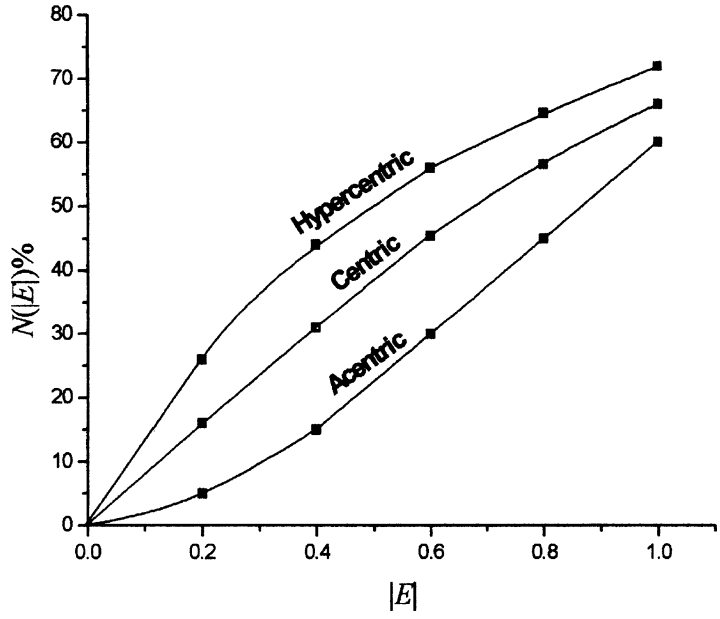

Fig. 4.10 Cumulative distributions $N(|E|)$. The region $0 < |E| < 1$ is the most discriminatory, as the curves tend to converge and actually cross over at higher values of |E|

4.3 Problems

4.1. An organic crystal has a large overall isotropic temperature factor of 6.8 Å^2. What is the percentage reduction of the atomic scattering factor of a carbon atom at room temperature for a reflection at $\theta = 27.55°$, with Cu $K\alpha$ radiation ($\lambda = 1.5418$ Å) compared to that for a carbon

$(\sin\theta)/\lambda$	f_C
0	6
0.1	5.108
0.2	3.560
0.3	2.494
0.4	1.948
0.5	1.686

atom at rest scattering under the same conditions? What is the root mean square amplitude of vibration of the atom in a direction normal to the given reflecting plane? How might the data collection process for this crystal be improved?

4.2. Calculate the ideal intensities, $|F|^2$, for the 111 and 222 reflections for NaCl and KCl. Hence, discuss these reflections in the light of Fig. 12.10. The necessary data are as follows: a (NaCl) = 5.627 Å, a (KCl) = 6.278; f values may be calculated from the equation $\sum_1^4 a_i \exp(-b_i s^2) + c_i$, where $s = (\sin\theta)/\lambda$, and the constants for the equation are listed below.

	a_1	b_1	a_2	b_2	a_3	b_3	a_4	b_4	c
Na^+	3.2565	2.6671	3.9362	6.1153	1.3998	0.2001	1.0032	14.0390	0.4040
K^+	7.9578	12.6331	7.4917	0.7674	6.3590	−0.0020	1.1915	31.9128	−4.9978
Cl^-	18.2915	0.0066	7.2084	1.1717	6.5337	19.5424	2.3386	60.4486	−16.3780

4.3. Show that, in the centric distribution, $M_c(=\overline{F}^2/\overline{F^2}) = 0.637$.
4.4. The value of $|\mathrm{E}|^3$ for the acentric distribution is 1.329. Find the value of $\overline{|\mathrm{E}|^3}$ for the centric distribution.
4.5. The value of $\overline{|E^2-1|}$ in the centric distribution has been shown to be 0.968. Find the corresponding value in the acentric distribution.
4.6. Compare the statistically distinguishable features of space groups Pm, $P2$, and $P2/m$ and work out a scheme for distinguishing between them.
4.7. How may one distinguish between the space groups that have the diffraction symbols (a) $mmm\ Pc**$ and (b) $mmm\ C***$?

References

1. See Bibliography, James (1958) International tables for X-ray crystallography, vol C. 2nd edn. (1999)
2. Zachariasen WH (1967) Acta Crystallogr 23:558
3. Busing WR, Levy HA (1957) Acta Crystallogr 10:180
4. Blessing RH (1995) Acta Crystallogr A51:33; idem J Appl Crystallogr 30:421 (1997)
5. Tickle IJ (1975) Acta Crystallogr B31:329
6. Wilson AJC (1942) Nature 150:152
7. See Bibliography, Ibers and Hamilton (1974)
8. Hall SR, Subramanian V (1982) Acta Crystallogr A38:590; idem ibid A38:598 (1982)
9. http://xtal.source.forge.net/man/genev-desc.html# 2776482
10. French S, Wilson K (1978) Acta Crystallogr A34:517
11. Robertson JM, White JG (1947) J Chem Soc 358
12. Carrell CJ et al (1997) Carcinogenesis 18:415
13. Rogers D, Wilson AJC (1953) Acta Crystallogr 6:439

Bibliography: Intensity and Intensity Statistics

James RW (1958) Optical principles of the diffraction of X-rays: the crystalline state, vol 2. Bell, London
Prince E, Wilson AJC (1999) International tables for X-ray crystallography, vol C, 2nd edn. Kluwer, London
Woolfson MM (1977) An introduction to X-ray crystallography, 2nd edn. Cambridge University Press, Cambridge